Oxidative Destruction of Hydrocarbons on a New Zeolite-like Crystal of $Ca_{12}Al_{10}Si_4O_{35}$ Including O_2^- and O_2^{2-} Radicals

Satoru Fujita,*,† Kenzi Suzuki,† Makio Ohkawa,‡ Toshiaki Mori,§ Yasuo Iida,† Youhei Miwa,|| Hideki Masuda,|| and Shigetaka Shimada||

Ceramic Research Institute, National Institute of Advanced Industrial Science and Technology, 2266-98 Anagahora, Shimoshidami, Moriyama-ku, Nagoya 463-8560, Japan, Department of Earth and Planetary Sciences, Faculty of Science, Hiroshima University, Higashi-Hiroshima, Hiroshima 739-8526, Japan, Department of Materials Science and Technology, Faculty of Science and Technology, Hirosaki University, 3, Bunkyo-cho, Hirosaki 036-8561, Japan, and Department of Materials Science and Engineering, Faculty of Engineering, Nagoya Institute of Technology, Gokiso-cho, Showa-ku, Nagoya 466-8555, Japan

Received April 23, 2002. Revised Manuscript Received October 30, 2002

To develop a nonmetal catalyst to decompose hydrocarbons, a new zeolite-like $Ca_{12}Al_{10}Si_4O_{35}$ was prepared by calcining hydrogarnet, $Ca_3Al_2(SiO_4)_{0.8}(OH)_{8.8}$, a hydrothermal reaction product from a mixture of CaO, Al_2O_3 sol, and amorphous SiO_2. The X-ray diffraction analysis showed the framework of $(Al,Si)O_4$ tetrahedra formed in the $Ca_{12}Al_{10}Si_4O_{35}$ crystal. ESR measurement and Raman spectroscopy revealed that both superoxide anions (O_2^-) and peroxide species (O_2^{2-}) existed in the cavity of the framework. Due to the O_2^- and O_2^{2-} species present, $Ca_{12}Al_{10}Si_4O_{35}$ exhibited high activity for the oxidation of hydrocarbons to carbon oxides (CO_2 and CO) and H_2O at >400 °C.

Introduction

Over the past several years, environmental legislation has imposed increasingly stringent limits for permitted atmospheric emission levels. In particular, the release of hydrocarbons, especially, volatile organic compounds (VOCs), has been highly limited. VOCs are a wide-ranging class of chemicals derived from many sources and consist of over 300 compounds.[1] In view of the magnitude of the problem presented to the chemical and processing industries, the major challenge they face is to reduce the emission of pollutants without stifling economic growth. Abatement technologies to control the release of hydrocarbons to the environment are therefore of paramount importance. The most widely adopted technique is thermal combustion, which requires temperatures >1000 °C, and further, the use of a metal oxide as a catalyst, such as that of cobalt, copper, manganese, and so on, significantly lowers the process operating temperature range to 300−600 °C.[2−4] However, those catalysts are costly and limited in view of natural resources. Therefore, an attractive catalyst involves the use of nonmetal materials that can completely oxidize hydrocarbons. The development of nonmetal oxide catalysts active for the combustion of a wide range of hydrocarbons is a major challenge for future research. The aim of this study is to examine the combustion activity of $Ca_{12}Al_{10}Si_4O_{35}$ for various kinds of hydrocarbons (benzene, chlorobenzene, toluene, and propylene). $Ca_{12}Al_{10}Si_4O_{35}$ is known as a material with the ability for fixation of anions such as chloride ion at high temperatures.[5] Technology to remove exhaust gases by using $Ca_{12}Al_{10}Si_4O_{35}$ may suppress a side reaction, which leads to the formation of polychlorinated dibenzo-*p*-dioxins (PCDDs) and dibenzofurans (PCDFs) via *de novo* synthesis in the municipal waste incineration process.[6]

Experimental Section

Preparation of $Ca_{12}Al_{10}Si_4O_{35}$. $Ca_{12}Al_{10}Si_4O_{35}$ was formed by heating hydrogarnet [$Ca_3Al_2(SiO_4)_{0.8}(OH)_{8.8}$] at 800 °C. The hydrogarnet was hydrothermally synthesized from a stoichiometric mixture of alumina sol, amorphous silica, and calcium oxide. The mixture was placed in a Teflon-lined stainless steel autoclave (25-mL volume) with distilled water and then heated with rotation at 50 rpm. The water-to-solid weight ratio was 12:1. The autoclave was placed in a temperature-controlled oven, the temperature of which was increased from room temperature to 200 °C in 2 h. The mixture then was kept at 200 °C for 15 h. The solid products were separated by filtration and dried at 110 °C for 24 h.

* To whom correspondence should be addressed. Tel.: 81-52-736-7258. E-mail: fujita-sato@aist.go.jp.
† National Institute of Advanced Industrial Science and Technology.
‡ Hiroshima University.
§ Hirosaki University.
|| Nagoya Institute of Technology.

(1) Mukhopadhyay, N.; Moretti, E. C. *Current and potential future industrial practices for controlling volatile organic compounds*; Center For Waste Control Management, 1993.
(2) Kang, Y. M.; Wan, B. Z. *Appl. Catal., A* **1994**, *114*, 35.
(3) Drago, R. S.; Jurczyk, K.; Singh, D. L.; Young, V. *Appl. Catal., B* **1996**, *8*, 155.
(4) Watanabe, N.; Yamashita, H.; Miyadera, H.; Tominaga, S. *Appl. Catal., B* **1996**, *8*, 405.
(5) Fujita, S.; Suzuki, K.; Ohkawa, M.; Shibasaki, Y.; Mori, T. *Chem. Mater.* **2001**, *13*, 2523.
(6) Stieglitz, L.; Zwick, G.; Beck, J.; Bautz, H.; Roth, W. Carbonaceous Particles In Fly Ash -A Source For the DE-NOVO−Synthesis of Organochlorocompounds. *Chemosphere* **1989**, *19*, 283.

10.1021/cm0204122 CCC: $25.00
Published on Web 12/13/2002

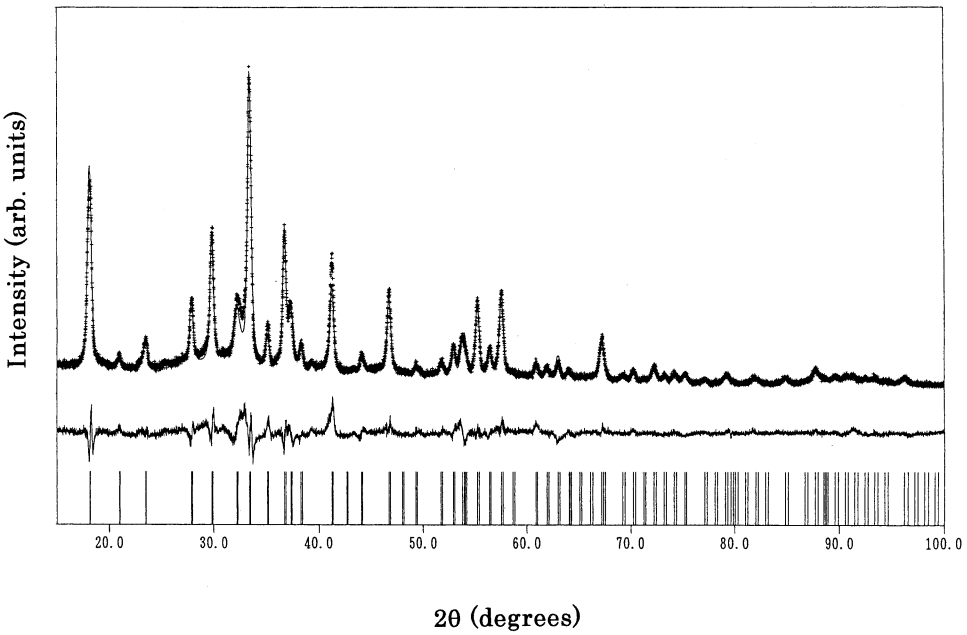

Figure 1. Rietveld refinement pattern of $Ca_{12}Al_{10}Si_4O_{35}$. Plus signs (+) represent the observed data and the solid line indicates the calculated pattern. A difference (obsd−calcd) plot is shown beneath.

Characterization. The X-ray powder diffraction data were obtained with an M18XHF diffractometer (MAC Science, Ltd.) using Ni-filtered Cu Kα radiation (40 kV, 100 mA). The diffraction pattern was collected immediately after cooling the sample from 800 °C to room temperature over a diffraction angle range from 10 to 100° with a 2θ step increment of 0.01° and a counting time of 1.2 s for each step. The crystal structure refinement was carried out by the Rietveld method using the program REITAN 94,[7] dealing with a sample consisting of two phases ($Ca_{12}Al_{10}Si_4O_{35}$ and CaO). Diffraction peak profiles were modeled using a pseudo-Voigt function corrected for asymmetry, and the background was modeled using Legendre polynomials with eight coefficients. The refinement was initiated with the positional parameters of $Ca_{12}Al_{14}O_{33}$.[8] The occupancy parameters were fixed assuming that the Ca, T(1), and T(2) sites were occupied by Ca, Al, and $Al_{1/3}Si_{2/3}$, respectively. Equivalent isotropic atomic displacement parameters of T(1) and T(2) and of O(1), O(2), and O(3) were constrained to have the same values, respectively. The surface area was measured by N_2 adsorption−desorption equipment at 77 K (Bell Japan, BELSORP 28SP). The Raman spectroscopy experiment was carried out using a spectrometer (SPEX, 1877) with the 514.5-nm line of an Ar^+ laser for excitation, and about 100 mW of power was focused on the sample. The spectrum was recorded by a liquid-nitrogen-cooled change-coupled device (CCD) detector (Prinston Instruments, LN/CCD-1100PB) over a scanning range of 790−1150 cm^{-1}.

Oxidation of Hydrocarbons. The oxidation of hydrocarbons was performed using a conventional flow-type microreactor of quartz glass in the range from room temperature to 800 °C. Synthetic air (80% N_2 and 20% O_2) was used. The concentration of hydrocarbons (benzene, mono-chlorobenzene, and toluene) was adjusted to 1000 ppmv by bubbling air through a temperature-controlled impinger. The total gas flow was 100 mL/min and the space velocity was 10 000 h^{-1}. The catalyst was sieved to a size of 300−500 μm and placed in the reactor between silica wool. The effluent gases were analyzed by an on-line gas chromatograph (Shimadzu, Gas Chromatograph GC-8A) with Porapak P for the organic compounds and active carbon for CO_2 and CO as a separation column. HCl and Cl_2 formed by the decomposition of chlorobenzene and by the Deacon reaction, respectively, were absorbed by bubbling the effluent gases through 0.1 N NaOH solution before analyzing by gas chromatography.

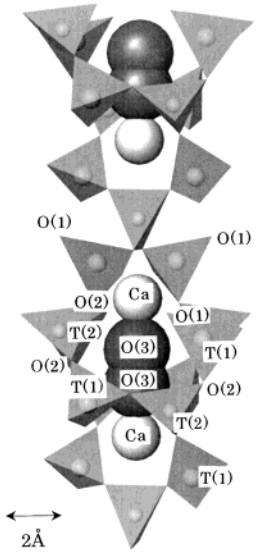

Figure 2. Crystal structure of $Ca_{12}Al_{10}Si_4O_{35}$, showing the links of tetrahedra. The large and small spheres represent O(3) and Ca ions, respectively.

Result and Discussion

$Ca_{12}Al_{10}Si_4O_{35}$ Crystal Structure. Figure 1 shows the X-ray powder diffraction pattern of the sample. The obtained $Ca_{12}Al_{10}Si_4O_{35}$ sample contains a minor amount of CaO, which indicates the phase transition from hydrogarnet to $Ca_{12}Al_{10}Si_4O_{35}$ according to the following equation (1):

$$5Ca_3Al_2(SiO_4)_{0.8}(OH)_{8.8} \rightarrow Ca_{12}Al_{10}Si_4O_{35} + 3CaO + 22H_2O \quad (1)$$

Figure 2 shows the crystal structure of $Ca_{12}Al_{10}Si_4O_{35}$. Tables 1 and 2 show the crystallographic data and

(7) Izumi, F. In *The Rietveld Method*; Young, R. A., Ed.; Oxford University Press: Oxford, U.K., 1993; Chapter 13.

Table 1. Crystallographic data for $Ca_{12}Al_{10}Si_4O_{35}$

Results of Rietveld Refinement	
cryst system	
a (Å)	11.9748(15)
V (Å^3)	1717
space group	$I\bar{4}3d$
Reliability Factors	
R_{wp}[a] (%)	11.26
R_p[b]	8.88
R_{expt}[c]	6.47
R_I[d]	5.70
R_F[e]	2.94
s[f]	1.74

[a] Weighted pattern R factor. [b] Pattern R factor. [c] Expected R factor. [d] Integrated intensity R factor. CaO: $R_I = 2.00\%$. [e] Structure factor R factor. CaO: $R_F = 1.07\%$. [f] Goodness-of-fit indicator (R_{wp}/R_{expt}).

Table 2. Atomic Positions for $Ca_{12}Al_{10}Si_4O_{35}$

atom	x	y	z	occu. factor	thermal param. (Å^2)
Ca	0.1034(11)	0	1/4		1.50(58)
T(Al)	−0.0183(11)	−0.0183	−0.0183		1.19(58)
T(Al, Si)	3/8	0	1/4		1.19
O(1)	0.0593(26)	0.0593	0.0593		1.23(69)
O(2)	0.0381(17)	0.0543	0.6538(23)		1.23
O(3)	0.0754(62)	1/2	1/4	0.39(3)	1.23

Table 3. Interatomic Distances (Å) for $Ca_{12}Al_{10}Si_4O_{35}$

	Ca Decahedron		
	Ca−O(1)	2.44(3) ×2	
	Ca−O(2)	2.38(2) ×2	
	Ca−O(2)	2.57(2) ×2	
	Ca−O(3)	2.14(7)	
	mean	2.42	
O(1)−O(2)	2.90(5) ×3	O(2)−O(1)	2.90(5)
O(1)−O(2)	3.22(6) ×3	O(2)−O(2)	2.79(4)
O(1)−O(3)	2.88(4) ×3	O(2)−O(2)	2.81(4) ×2
		O(2)−O(3)	3.15(4)
O(3)−O(3)	1.19(15)	O(2)−O(1)	3.22(4)
	T(Al) Tetrahedron		
T(Al)−O(1)	1.61(5)	O(1)−O(2)	2.90(5)
T(Al)−O(2)	1.81(2) ×3	O(2)−O(2)	2.79(4)
mean	1.76		
	T(Al,Si) Tetrahedron		
T(Al,Si)−O(2)	1.68(2) ×4	O(2)−O(2)	2.79(4)
mean	1.68	O(2)−O(2)	2.81(4)

atomic positions for $Ca_{12}Al_{10}Si_4O_{35}$, respectively. The crystal structure of $Ca_{12}Al_{10}Si_4O_{35}$ is the same as that of mayenite [$Ca_{12}Al_{14}O_{33}$].[8−11] We suppose that Si^{4+} preferentially occupies the T(2) site like other mayenite-related compounds.[12−14] Because of the substitution of Si^{4+} in the T(2) site, the T(2)−O mean distance (1.68 Å) is shorter than that of T(1)−O (1.76 Å) (see Table 3). The bond valence sum[15] of T(1) is 3.07, while that of T(2) is 3.50, which is far from 3.00 because of substituting Si^{4+} in the T(2) site. Two tetrahedra, T(1) and T(2), link together to form the framework structure. The Ca polyhedron consists of two O(1), four O(2), and single O(3) anions. O(3) is located in the cavity of the framework, statistically. The occupancy of O(3) reckoned from the chemical formulas is 0.25 (3 atoms per formula unit). It should be emphasized that the number is 3 times larger than that of mayenite [$Ca_{12}Al_{14}O_{33}$] in which the O(3) site is occupied statistically by 1 atom per formula unit. The bond valence sums of O(1), O(2), and O(3) are 1.94, 2.04, and 0.62, respectively, and those of O(1) and O(2) constituting the T(1) and T(2) tetrahedrals are close to 2.00 (O^{2-}), and further, those of O(3) imply that O(3) is not O^{2-}.

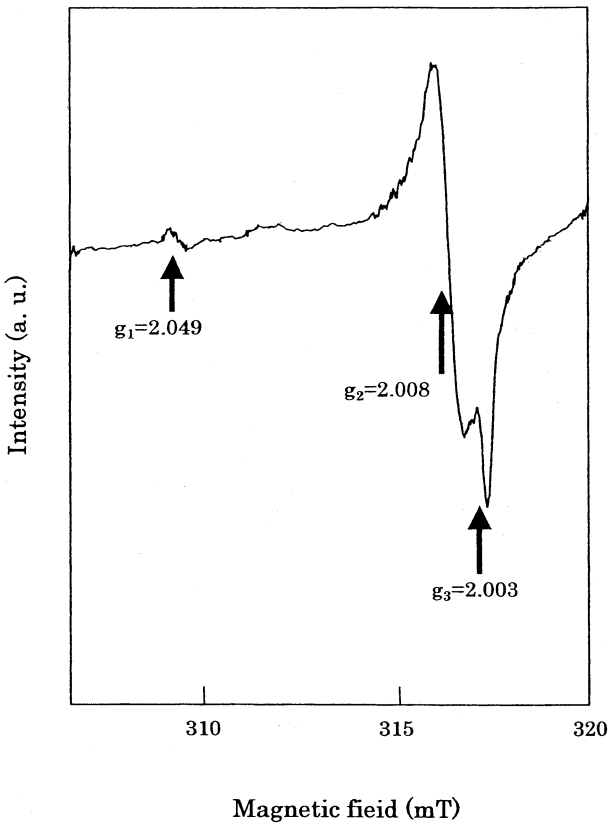

Figure 3. ESR spectrum of $Ca_{12}Al_{10}Si_4O_{35}$ measured at 300 K.

Figure 3 shows the ESR spectrum of $Ca_{12}Al_{10}Si_4O_{35}$ with an asymmetric shape. The magnetic field was calibrated with a proton resonance marker. On the basis of the close agreement of the set of g values obtained here with those in the literature,[16−18] especially on a characteristic g_1 far from 2.00, the signal observed can be attributed to the superoxide radical anion O_2^-. Figure 4 shows the Raman spectra of $Ca_{12}Al_{10}Si_4O_{35}$. The spectra were scanned in the range of 790−1150 cm^{-1} with a resolution of 2 cm^{-1} at room temperature. The molecular O_2 species has been assigned to a band at 1556 cm^{-1}; superoxide (O_2^-) and peroxide (O_2^{2-}) species are observed at 1015−1180 and 640−970 cm^{-1}, respectively.[19−22] In the present study, the O_2^- and O_2^{2-} species are observed at 1075 and 853 cm^{-1}, respectively,

(8) Bartl, H.; Scheller, T. *Neues Jahrb. Mineral. Monatsh.* **1970**, *35*, 547.
(9) Williams, P. P. *Acta Crystallogr., Sect. B: Struct. Sci.* **1973**, *29*, 1550.
(10) Hosono, H.; Abe, Y. *Inorg. Chem.* **1987**, *26*, 1192.
(11) Lacerda, M.; Irvine, J. T. S.; Glasser, F. P.; West, A. R. *Nature* **1988**, *332*, 525.
(12) Tsukimura, K.; Knazawa, Y.; Aoki, M.; Bunno, M. *Acta Crystallogr., Sect. C: Cryst. Struct. Commun.* **1993**, *49*, 205.
(13) Kanazawa, Y.; Aoki, M.; Takeda, H. *Bull. Geol. Surv. Jpn.* **1997**, *48*, 413.
(14) Feng, Q. L.; Glasser, F. P.; Howie, R. A.; Lachowski, E. E. *Acta Crystallogr., Sect. C: Cryst. Struct. Commun.* **1988**, *44*, 589.
(15) Brese, N. E.; O'Keeffe, M, *Acta Crystallogr., Sect. B: Struct. Sci.* **1991**, *47*, 192
(16) Brown, I. D.; Brown D. Altermatt, *Acta Crystallogr., Sect. B: Struct. Sci.* **1985**, *41*, 244.
(17) Lunsford, J. H. *Catal. Rev.* **1973**, *8* (1), 135.
(18) Che, M.; Tench, A. J. *Adv. Catal.* **1983**, *32*, 1.
(19) Hayashi, K.; Hirano, M.; Matsuishi, S.; Hosono, H. *J. Am. Chem. Soc.* **2002**, *124* (5), 738.

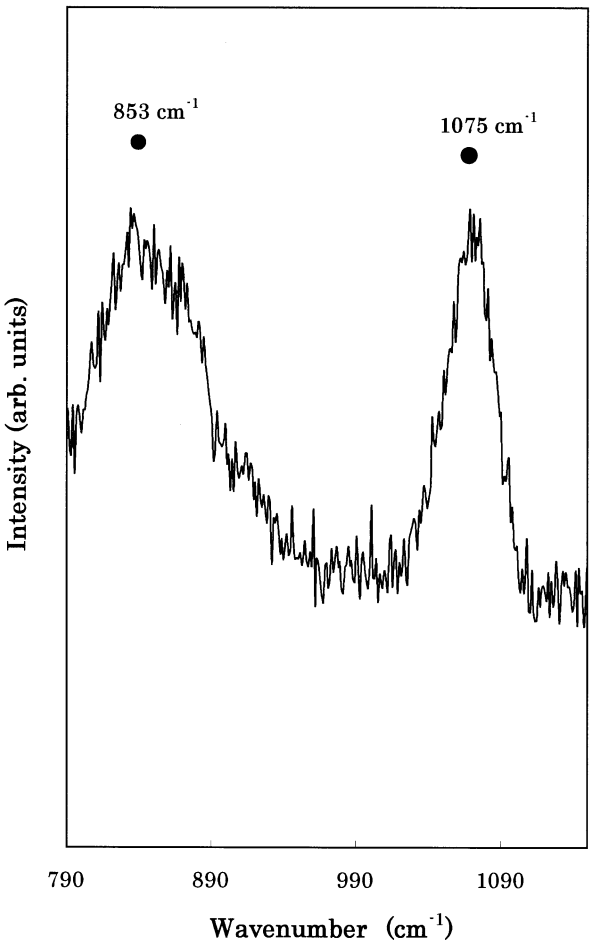

Figure 4. Raman spectrum of $Ca_{12}Al_{10}Si_4O_{35}$ measured at 300 K.

Table 4. BET Surface Area (m^2/g)

hydrogarnet	after heating hydrogarnet
43	7

corresponding to the stretching vibration frequency. It is concluded that the O_2^- and O_2^{2-} are involved in the structural cavity inherent in the crystal lattice. Because only 32 oxygens in the formula unit belong to the aluminosilicate framework, the formula of $Ca_{12}Al_{10}Si_4O_{35}$ should be expressed as $Ca_{12}(Al_{10}Si_4O_{32})O_3$ to emphasize the incorporated superoxide and peroxide.

Figure 5 shows a Fourier map on the horizontal section at $Z = 0.75$ obtained from Rietveld analysis. Two high electron density peaks were observed between Ca atoms. There are two possible interpretations: one is that one of the two sites is statistically occupied and/or the other is that O_2^- or O_2^{2-} occupies these sites. In the case where the two sites are simultaneously occupied, the interatomic distance of O(3)−O(3) is 1.19 Å and is short in comparison with those of oxygen molecules (O_2^-, 1.33 Å; O_2^{2-}, 1.49 Å). A large cavity in the framework of the $(Al,Si)O_4$ tetrahedra accommodates linearly coordinated Ca−O(3)−O(3)-Ca atoms. Therefore, the short O(3)−O(3) distance may be restricted by the Ca−O(3) distance (2.14 Å). The bond valence sum assigned to the two O(3) sites is 1.25 (0.62 × 2) and implies that the molecular oxygen of O(3)−O(3) exists as a species of both O_2^- and O_2^{2-}. The refined site

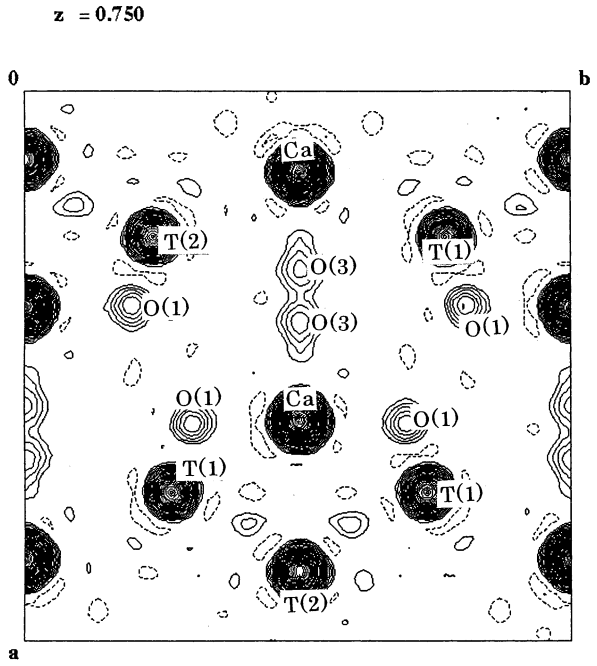

Figure 5. Fourier map of $Ca_{12}Al_{10}Si_4O_{35}$ structure at $z = 0.75$. The map was calculated using Rietveld-derived observed Bragg intensities. The contour interval is 1.0 $e^-/Å^3$.

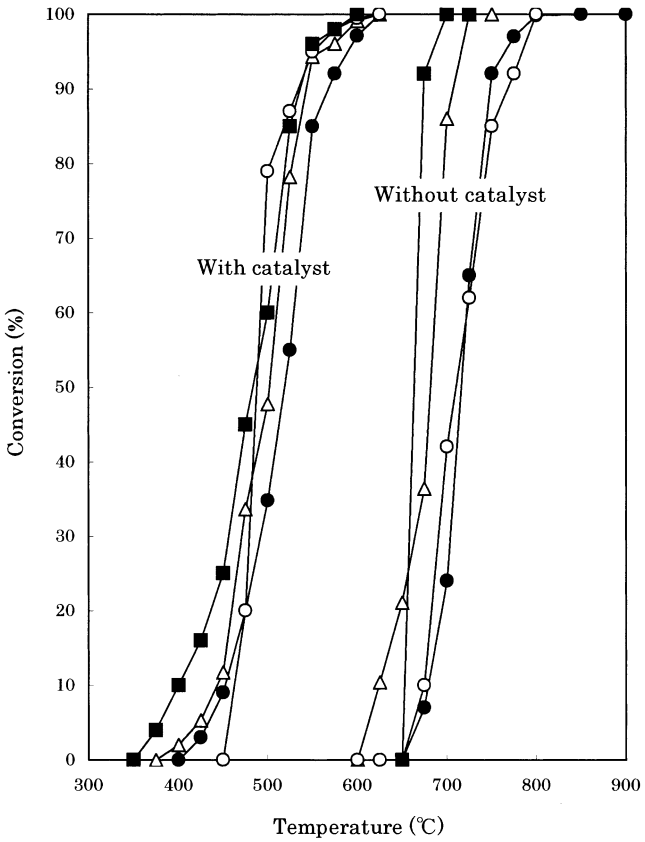

Figure 6. The oxidation curves for various hydrocarbons over $Ca_{12}Al_{10}Si_4O_{35}$: ●, benzene; ○, chlorobenzene; ■, toluene; △, propylene.

(20) Shamir, J.; Binenboym, J.; Classen, H. W. *J. Am. Chem. Soc.* **1968**, *90*, 6223.
(21) Giamello, E.; Sojka, Z.; Che, M.; Zecchina, A. *J. Phys. Chem.* **1986**, *90*, 6084.
(22) Metcalfe, A.; Shankar, S. *J. Chem. Soc., Faraday Trans. 1* **1980**, *76*, 630.

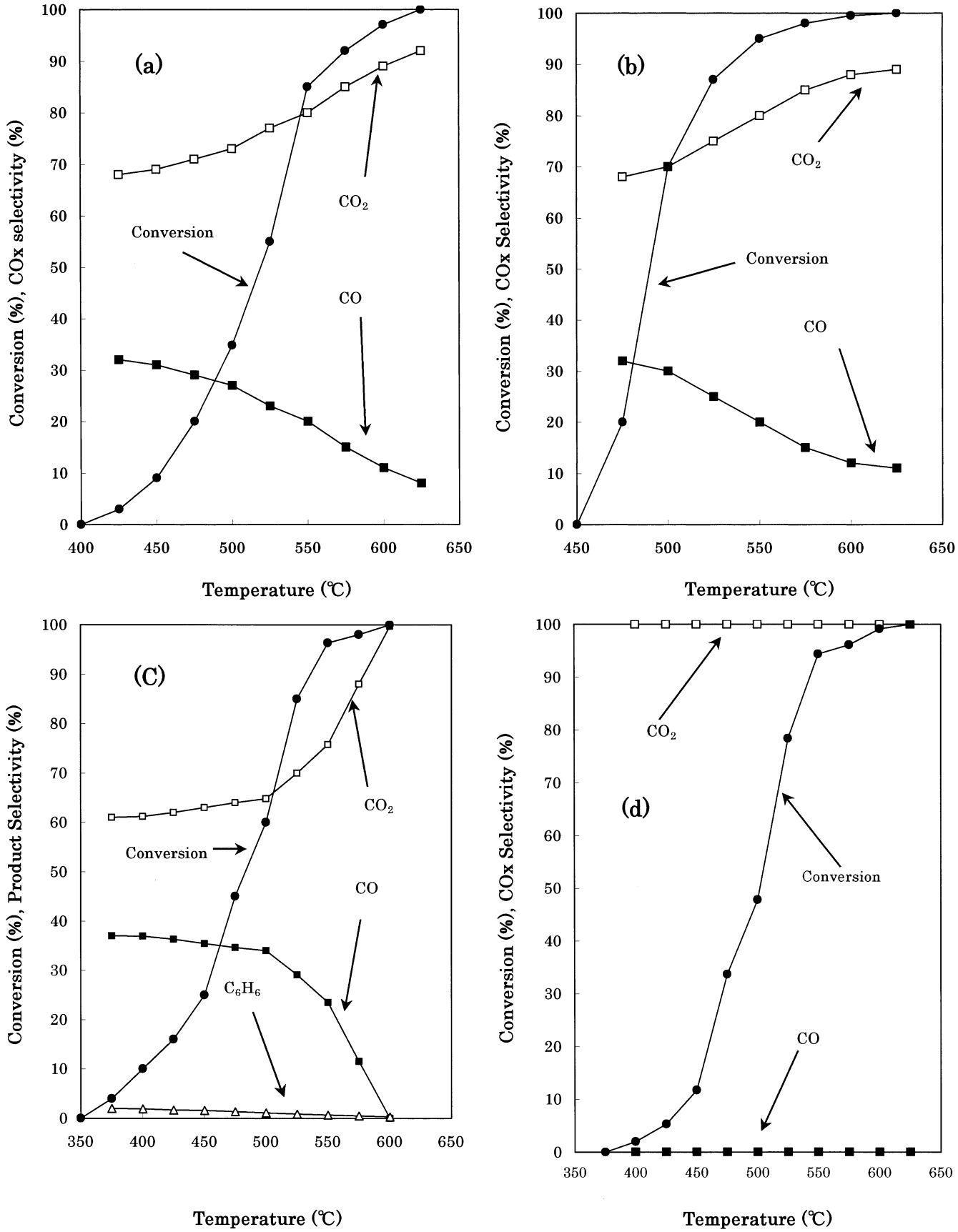

Figure 7. Conversion and carbon oxide selectivity for each hydrocarbon at various temperatures using $Ca_{12}Al_{10}Si_4O_{35}$: (a) benzene; (b) chlorobenzene; (c) toluene; (d) propylene.

occupancy factor of the O(3) obtained from Rietveld analysis is 0.39(4). The empirical formula obtained from the site occupancy factor can be indicated as $[Ca_{12}Al_{10}Si_4O_{32}]^{6+}[O_{4.7}]^{6-}$. Assuming that every O(3) is an oxygen

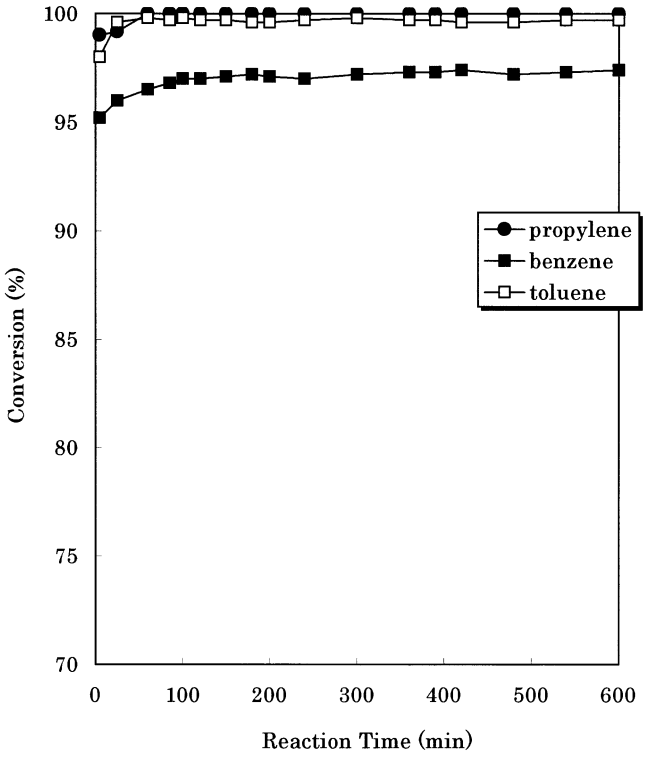

Figure 8. Activity tests for 1000 ppm various hydrocarbons (at 600 °C, SV = 10 000 h^{-1}) over $Ca_{12}Al_{10}Si_4O_{35}$: ■, benzene; □, toluene; ●, propylene.

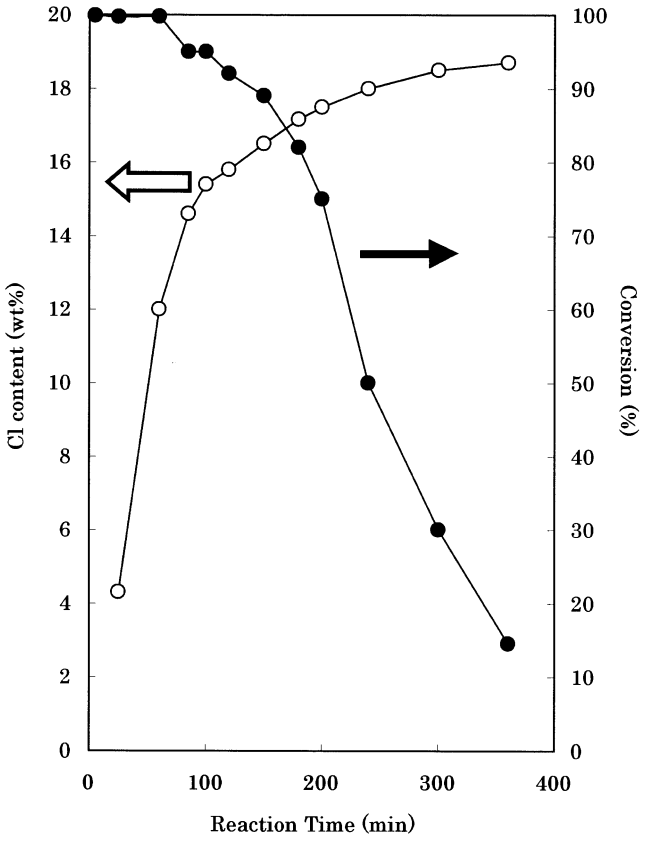

Figure 9. Relationship between conversion for chlorobenzene and chlorine contents of $Ca_{12}Al_{10}Si_4O_{32}Cl_6$ and $CaCl_2$ under 1% chlorobenzene, SV = 10 000 h^{-1} and 600 °C using $Ca_{12}Al_{10}Si_4O_{35}$.

radical, the charge valence cannot be compensated. The shortage indicates that several O^{2-} ions occupy the O(3) site and/or the content of the Si ion might be lower than that expected from the formula.

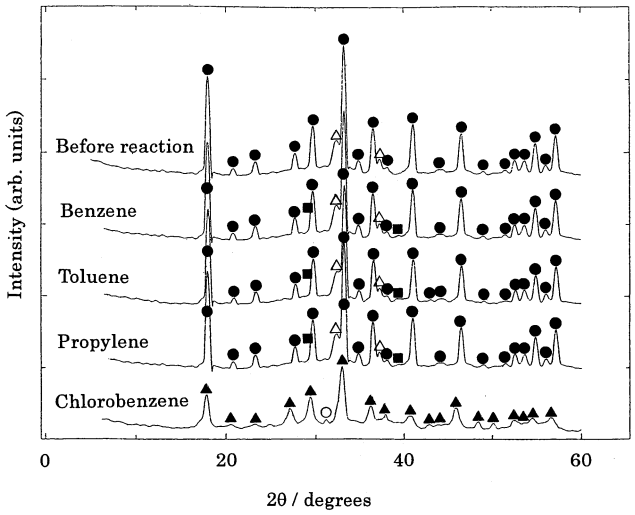

Figure 10. XRD patterns of catalysts before and after reaction with various hydrocarbons at 600 °C: ●, $Ca_{12}Al_{10}Si_4O_{35}$; △, CaO; ■, $CaCO_3$; ▲, $Ca_{12}Al_{10}Si_4O_{32}Cl_6$; ○, $CaCl_2 \cdot 2H_2O$.

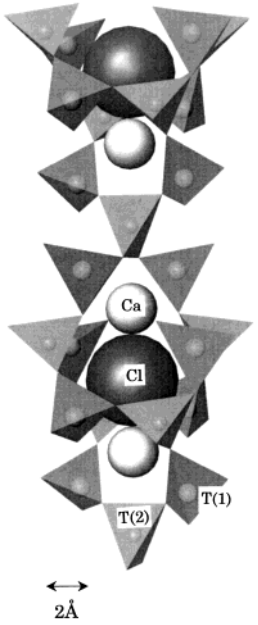

Figure 11. Crystal structure of $Ca_{12}Al_{10}Si_4O_{32}Cl_6$, showing the links of tetrahedra. The large and small spheres represent chloride and calcium ions, respectively.[5]

Oxidation of Hydrocarbons. Table 4 summarizes the BET surface areas of the powder sample before and after calcining at 800 °C. Although the uncalcined sample exhibits a significantly large surface area, the value (7 m^2/g) is very low for the calcined sample. The conversion of hydrocarbons to CO_2 and/or CO is plotted in Figure 6 as a function of the reaction temperature. With the catalyst, the oxidation begins at around 400 °C and is completed at 625, 625, 600, and 625 °C for benzene, chlorobenzene, toluene, and propylene, respectively, while the respective temperatures for complete oxidation are 800, 800, 700, and 725 °C without the catalyst (packed with only fragmented quartz glass). A considerable amount of CO is produced except for the oxidation of propylene. The selectivity for CO and CO_2,

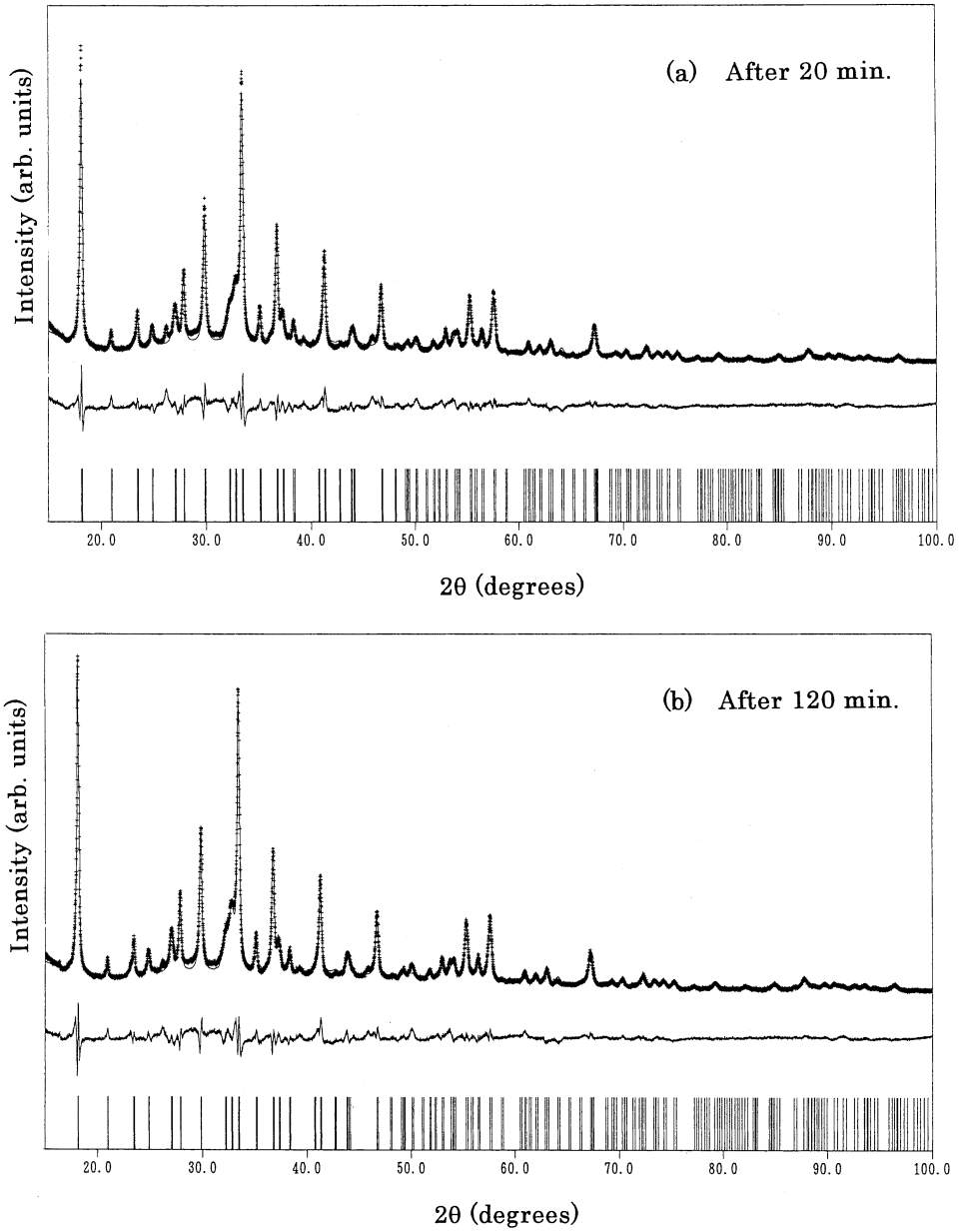

Figure 12. Rietveld refinement pattern of $Ca_{12}Al_{10}Si_4O_{35}$ after reacting with propylene for 20 min (Figure 13a) and 120 min (Figure 13b) at 600 °C. Plus signs (+) represent the observed data and the solid line indicates the calculated pattern. A difference (obsd−calcd) plot is shown beneath.

calculated from the following equations, is displayed in Figure 7.

$$S_{CO} = CO/(CO + CO_2) \times 100\ (\%)$$

$$S_{CO_2} = CO_2/(CO + CO_2) \times 100\ (\%)$$

The values of CO selectivity decrease with increasing temperature for benzene, chlorobenzene, and toluene. A trace amount of benzene is also produced from the toluene oxidation. Figure 8 displays the conversions of benzene, toluene, and propylene for a long time at 600 °C. Stable activity is observed for the oxidation of all these hydrocarbons. For chlorobenzene, on the other hand, the conversion dramatically decreases after the initial stable reaction period, as shown in Figure 9. The cumulative amount of chlorine is also plotted in Figure 9 as a function of the reaction time. In harmony with the decrease in the conversion of chlorobenzene, the value significantly increases followed by a very mild increase to ≈19 wt % after the reaction for 360 min. The XRD patterns after the reaction of each hydrocarbon are illustrated in Figure 10. Although a calcite phase was partially formed by reaction between CaO and CO_2 generated after the oxidations of benzene, toluene, and propylene, new XRD patterns attributed to wadalite ($Ca_{12}Al_{10}Si_4O_{32}Cl_6$)[12,13] and to $CaCl_2 \cdot 2H_2O$ appeared for the reaction of chlorobenzene. The theoretical chlorine content for the mixture of $Ca_{12}Al_{10}Si_4O_{32}Cl_6$ and $CaCl_2$ was 22.1 wt %, which explained the observed chlorine content of 19 wt %. The structure of $Ca_{12}Al_{10}Si_4O_{32}Cl_6$ is shown in Figure 11.[5] It is considered that the formation of $Ca_{12}Al_{10}Si_4O_{32}Cl_6$ results from the exchange of oxygen species in the cavity of the $Ca_{12}Al_{10}Si_4O_{35}$ framework at >400 °C between O_2^- and Cl^- and/or between O_2^{2-} and $2Cl^-$. Therefore,

Table 5. Crystallographic Data for $Ca_{12}Al_{10}Si_4O_{35}$ after Reacting with Propylene under Inert Conditions

	before	after 20 min	after 120 min
a (Å)	11.9748(15)	11.9623(9)	11.9661(8)
V (Å^3)	1717	1711	1713
space group	$I\bar{4}3d$	$I\bar{4}3d$	$I\bar{4}3d$
	Reliability Factors		
R_{wp}[a] (%)	11.26	9.25	9.21
R_p[b]	8.88	7.38	7.48
R_{expt}[c]	6.47	3.50	3.51
R_I[d]	5.70	7.24	6.72
R_F[e]	2.94	4.48	4.07
s[f]	1.74	2.63	2.62
CaO R_I[d]	2.00	3.70	3.60
CaO R_F[e]	1.07	1.89	1.87
$CaCO_3$ R_I[d]		6.79	6.17
$CaCO_3$ R_F[e]		3.19	2.71

[a] Weighted pattern R factor. [b] Pattern R factor. [c] Expected R factor. [d] Integrated intensity R factor. [e] Structure factor R factor. [f] Goodness-of-fit indicator (R_{wp}/R_{expt}).

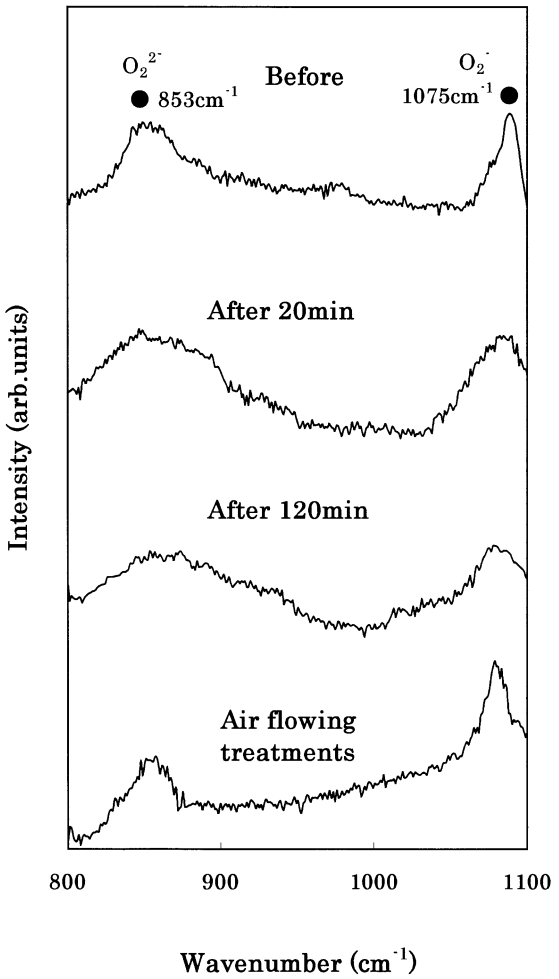

Figure 13. Raman spectra of $Ca_{12}Al_{10}Si_4O_{35}$ before and after reacting with propylene.

$Ca_{12}Al_{10}Si_4O_{35}$ has both the ability to oxidize hydrocarbons and to fix chloride ion in the cavity of the framework. By measuring the conversion of propylene over $Ca_{12}Al_{10}Si_4O_{32}Cl_6$ and $Ca_{12}Al_{10}Si_4O_{35}$ without gaseous oxygen, it was obvious that propylene hardly reacted on $Ca_{12}Al_{10}Si_4O_{32}Cl_6$. When $Ca_{12}Al_{10}Si_4O_{35}$ was used, on the other hand, propylene was decomposed; therefore, CO_2 was observed by oxidation. The quantity of CO_2 formed by combustion decreased with the decreasing decomposition activity of propylene.

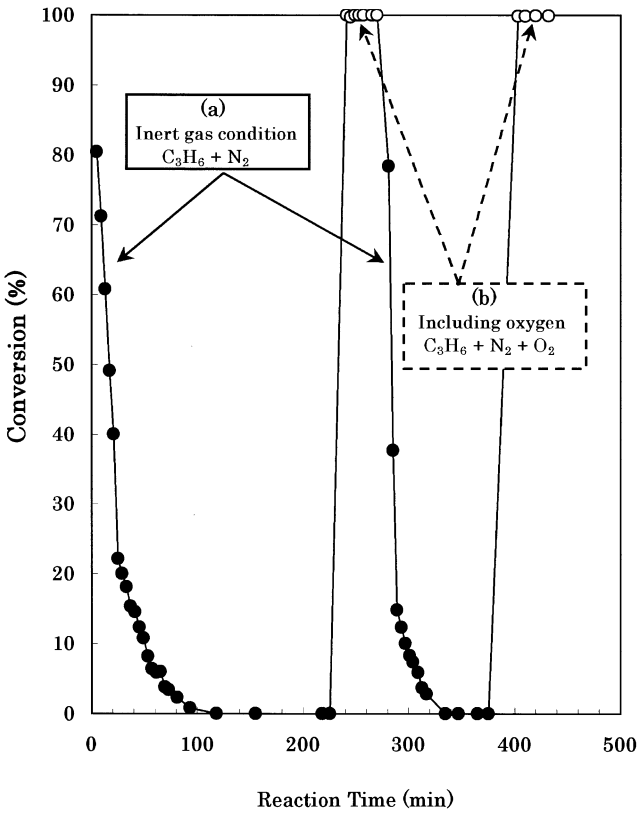

Figure 14. Recovery of the oxidation activity of $Ca_{12}Al_{10}Si_4O_{35}$ for 100 ppm propylene under inert (a) and including oxygen (b) conditions at 600 °C and SV = 1000 h^{-1}.

Table 6. Atomic Positions and Occupancy Factors of O(3) for $Ca_{12}Al_{10}Si_4O_{35}$ after Reacting with Propylene under Inert Conditions

atom	x	y	z	occu. factor	thermal param (Å^2)
		Before			
Ca	0.1034(11)	0	1/4		1.50(58)
T(Al)	−0.0183(11)	−0.0183	−0.0183		1.19(58)
T(Al,Si)	3/8	0	1/4		1.19
O(1)	0.0593(26)	0.0593	0.0593		1.23(69)
O(2)	0.0381(17)	0.0543(19)	0.6538(23)		1.23
O(3)	0.0754(62)	1/2	1/4	0.39(3)	1.23
		After 20 min			
Ca	0.0996(10)	0	1/4		1.23(57)
T(Al)	−0.0177(11)	−0.0177	−0.0177		0.80(57)
T(Al,Si)	3/8	0	1/4		0.80
O(1)	0.0586(26)	0.0586	0.0586		1.52(78)
O(2)	0.0340(17)	0.0532(18)	0.6548(21)		1.52
O(3)	0.0872(96)	1/2	1/4	0.29(3)	1.52
		After 120 min			
Ca	0.1000(10)	0	1/4		1.28(54)
T(Al)	−0.0175(10)	−0.0175	−0.0175		0.76(54)
T(Al,Si)	3/8	0	1/4		0.76
O(1)	0.0585(25)	0.0585	0.0585		1.47(66)
O(2)	0.0341(16)	0.0531(17)	0.6536(19)		1.47
O(3)	0.0859(97)	1/2	1/4	0.27(3)	1.47

Crystal structure refinement by the Rietveld method was also carried out for specimens after reaction dealing with the sample consisting of three phases ($Ca_{12}Al_{10}Si_4O_{35}$, μ-$CaCO_3$, and CaO). XRD patterns are shown in Figure 12 (a, after the reaction for 20 min; b, for 120 min). The crystallographic data and atomic positions of $Ca_{12}Al_{10}Si_4O_{35}$ are summarized in Tables 5 and 6, respectively. XRD analysis shows that the value of a is smaller after reaction than before reaction (see Table 5) and that the refined site occupancy factor of O(3) (Table 6) decreases with the reaction time from 0.39 to

0.27. These observed changes should result from the missing O_2^- and O_2^{2-} species from the $Ca_{12}Al_{10}Si_4O_{35}$ crystal. The Raman spectra of $Ca_{12}Al_{10}Si_4O_{35}$ before and after reaction are illustrated in Figure 13. The absorptions due to the O_2^- and O_2^{2-} species disappear with the progressing reaction, which supports the conclusion from the Rietveld analyses. The recovery of the oxidation activity of $Ca_{12}Al_{10}Si_4O_{35}$ was examined by supplying oxygen to the reactant, and this result is shown in Figure 14. Without gaseous oxygen, propylene conversion decreases to zero with time on stream, but the complete oxidation of propylene to CO_2 occurs after the introduction of oxygen to the reactant gas flow. The propylene conversion again decreases when gaseous oxygen is not supplied. The oxidation activity can be completely restored by supplying oxygen to the reactant gases, and furthermore, the absorptions of radical oxygen after the air flow treatments with a catalyst are observed from the Raman spectrum in Figure 13. Therefore, it is concluded that the O_2^- and O_2^{2-} species are readily lost to help decompose hydrocarbons and that they are readily restored in the lattice in the presence of gaseous oxygen.

Conclusions

A new phase, $Ca_{12}Al_{10}Si_4O_{35}$, forms a zeolitic structure with the framework of the $(Al,Si)O_4$ tetrahedra occluding the superoxide anion (O_2^-) and peroxide species (O_2^{2-}) in a large cavity. This material will open a new route to pollution abatement such as the fixation of hydrogen chloride gas and the combustion of hydrocarbons in exhaust gases. Due to the O_2^- and O_2^{2-} species present, $Ca_{12}Al_{10}Si_4O_{35}$ exhibited high activity for the oxidation of hydrocarbons to carbon oxides. Further studies are necessary under realistic conditions to establish the feasibility and viability for the application of our methodology; they are currently in progress.

Acknowledgment. We are grateful to Dr. S. Velu (Pennsylvania State University) for helpful suggestions and discussions.

CM0204122